TRANSIENT AMPLIFICATION OF SHEAR ALFVEN WAVES
AND
CONCOMITANT DEVELOPMENT OF THE BALLOONING INSTABILITY

Y. Y. LAU
Ronald C. Davidson
Bertram Hui

PFC/JA-79-11
September, 1979

TRANSIENT AMPLIFICATION OF SHEAR ALFVEN WAVES

AND

CONCOMITANT DEVELOPMENT OF THE BALLOONING INSTABILITY

Y. Y. Lau and Ronald C. Davidson,

Massachusetts Institute of Technology
Cambridge, Massachusetts 02139

and

Bertram Hui,

Naval Research Laboratory
Washington, D.C. 20375

Making use of the ideal MHD description in a plasma slab model, we study the transient amplification of shear Alfven waves and their concomitant development into gravitational (ballooning) instabilities as the plasma pressure is increased. When applied to tokamak geometry, for $\beta < \beta_c/2$, it is found that the ballooning mode has a negligibly small influence on the evolution of the shear Alfven waves. (Here, β is the ratio of plasma pressure to magnetic pressure, $\beta_c = Rr_n/L_s^2$ is the critical beta, R is the major radius, r_n is the plasma density length scale, and L_s the magnetic shear length scale.) The ballooning effect becomes dominant, however, for $\beta \gtrsim (3/4)\beta_c$, and the instability exhibits very strong growth whenever $\beta \gtrsim 1.1\beta_c$.

I. INTRODUCTION

Magnetic fluctuations are believed to play an important role in the transport of energy in a magnetically confined plasma[1-7]. Much of the recent research in this area involves an eigenmode analysis of microtearing instabilities where various kinetic and nonlinear effects are taken into account[3,4,7]. These effects enter most significantly in the thin region (critical layer) where magnetic reconnection takes place. While these analyses may be regarded as promising when compared with experiment, it is possible that these eigenmode solutions may be modified quantitatively when other realistic effects (e.g. curvature, equilibrium flow, impurities, etc.) are included. An example of the sensitivity of the eigenmode solution to the precise treatment for a thin critical layer is the recent demonstration that unstable eigenmode solutions do not exist for the universal instability.[8-10]

On the other hand, the equivalent treatment by means of an initial-value problem, i.e., the analysis of the evolution of a wavepacket, has a tendency to deemphasize such sensitivity. Because of the mathematical complexity, the study of the evolution of a wavepacket is usually restricted to slab geometry and to highly simplified equilibrium profiles[6,11]. However, it yields valuable information on the transient amplification (if any) of a wavelet if the medium does not admit unstable eigenmode solutions. It also illustrates how such an initial disturbance develops into an unstable eigenmode solution if such a solution exists.

Lau has recently shown that shear Alfven wave magnetic fluctuations can amplify to large amplitudes transiently before they decay[6]. This

result was obtained by treating an initial-value problem within the framework of the ideal MHD equations. The interpretation of this transient growth is that magnetic ripples on different field lines propagate at their respective local Alfven speeds. As one magnetic ripple approaches another on a neighboring field line, the current filaments associated with these ripples are aligned in phase, thus leading to a temporary amplification of the magnetic fluctuations before they decay due to shear effects at large times. This asymptotic decay has often been attributed to phase mixing of the shear Alfven continuum[12-15]. It should be noted that such transient amplification of shearing wavelets is entirely analogous to that encountered in classical sheared hydrodynamic flow.[11]

There has also been considerable recent interest in ballooning instabilities in tokamaks[16-18]. These instabilities are driven by unfavorable magnetic field curvature. Ballooning instabilities can be excited only if the plasma pressure lies in a certain range[17,18]. Moreover, because shear Alfven waves are coupled to the ballooning modes as the plasma pressure is increased, it is natural to investigate how the shear Alfven waves described in the previous paragraph develop into ballooning instabilities. In addition, it is also of considerable interest to examine the influence of curvature effects on the transient amplification of shear Alfven waves.[6] The purpose of the present article is to examine these issues.

For simplicity, we make use of the ideal MHD description in a plasma slab model. An effective gravity field is used to simulate the magnetic field curvature. This effective gravity field is proportional to β, the ratio of plasma pressure to magnetic pressure. Within the context of

local theory, the onset of the ballooning instability occurs when β exceeds a critical value β_c.

The main results of our numerical study of the evolution of an initial wavepacket can be summarized as follows. In the limit $\beta \to 0$, the transient amplification of shear Alfven waves confirms the previous results.[6] For $\beta < \beta_c/2$, this transient amplification is not significantly altered. For $\beta \gtrsim 0.75\ \beta_c$, however, ballooning effects dominate the evolution of the shear Alfven waves, and substantial amplification is observed. Indeed, for $\beta \gtrsim 1.1\beta_c$, the initial shear Alfven waves develop into a highly unstable, localized, ballooning mode.

The governing equations for the evolution of the wavepacket are formulated in Section II, and numerical solutions are discussed in Section III.

II. THEORETICAL DESCRIPTION

We consider a collisionless plasma described by the ideal magneto-hydrodynamic (MHD) equations in slab geometry. It is assumed that the local equilibrium magnetic field is $\vec{B}_o = B_o(\hat{z} + \hat{x}y/L_s)$, where B_o is a constant, and L_s is the length scale characterizing the magnetic shear. For this slab model to simulate tokamak geometry, the unit vectors $\hat{z}$, $\hat{x}$, and $\hat{y}$, respectively, are directed locally in the toroidal direction, the poloidal direction, and the radial direction. The equilibrium plasma has mass density ρ_o with scale length r_n in the $\hat{y}$ direction. We assume that a gravitational force per unit mass $\vec{g} = g\hat{y}$ simulates the magnetic field curvature. Here, $g = v_i^2/R$, where v_i is the ion thermal velocity,

and R is the major radius of the torus. The plasma is assumed to have zero flow velocity in the equilibrium state.

We consider small perturbations about such an equilibrium, assuming that the plasma is incompressible and free of dissipation. The linearized ideal MHD equations are given by

$$\frac{\partial \vec{B}_1}{\partial t} = \nabla\times(\vec{v}_1 \times \vec{B}_0) \tag{1}$$

$$4\pi\rho_0 \frac{\partial \vec{v}_1}{\partial t} = -\nabla(\vec{B}_1\cdot\vec{B}_1) + (\vec{B}_1\cdot\nabla)\vec{B}_0 + (\vec{B}_0\cdot\nabla)\vec{B}_1 - \nabla p_1 - 4\pi\rho_1 g\hat{y} \tag{2}$$

$$\frac{\partial \rho_1}{\partial t} + \nabla\cdot(\rho_0 \vec{v}_1) = 0 \tag{3}$$

$$\nabla\cdot\vec{v}_1 = 0 \tag{4}$$

$$\nabla\cdot\vec{B}_1 = 0 \tag{5}$$

where $\vec{v}_1$, $\vec{B}_1$ and p_1 are the perturbed flow velocity, magnetic field, and plasma pressure, respectively. Introducing the displacement vector $\vec{\xi}_1$, where $\vec{v}_1 = \partial\vec{\xi}_1/\partial t$, we assume that the perturbations have the form $\xi_{1y}(r,\vec{t}) = \xi_{1y}(y,t)\exp(ik_x x + ik_z z)$, with a similar expression for B_{1y}.

The y component of Eq. (1) gives

$$B_{1y} = i(\vec{k}\cdot\vec{B}_o)\,\xi_{1y}, \tag{6}$$

where $\vec{k} \equiv \hat{x}k_x + \hat{z}k_z$. Operating on Eq. (2) with $\vec{\nabla}\times\vec{\nabla}\times$, and taking the y component of the resulting equation, we obtain

$$\frac{\partial^2}{\partial t^2}(\nabla^2 \xi_{1y}) = i \frac{v_A^2}{B_o^2}(\vec{k}\cdot\vec{B}_o)\nabla^2 B_{1y} - \frac{k^2 g}{r_n}\xi_{1y} \tag{7}$$

where use has been made of Eqs. (3) - (5). It has been assumed that the equilibrium density gradient enters only in the buoyancy term $-4\pi\rho_1 g\hat{y}$ in Eq. (2), and that ρ_1 is calculated from Eq. (3) with $\vec{\xi}_1\cdot\nabla\rho_o \cong -\xi_{1y}\rho_o/r_n$. In Eq. (7), v_A denotes the local Alfven speed $B_o/(4\pi\rho_o)^{1/2}$.

It is readily deduced from Eqs. (6) and (7) that the local dispersion relation is given by

$$\omega^2 = k_\parallel^2 v_A^2 - \frac{g}{r_n} \equiv k_\parallel^2 v_A^2 - \left(\frac{\beta}{\beta_c}\right)\frac{v_A^2}{L_s^2} \tag{8}$$

where $k_\parallel \equiv (\vec{k}\cdot\vec{B}_o)/B_o$, and

$$\beta \equiv v_i^2/v_A^2 , \quad \beta_c \equiv Rr_n/L_s^2 . \tag{9}$$

For $k_\parallel \simeq 1/L_s$, the local dispersion relation (8) shows that the onset of ballooning instability occurs for $\beta > \beta_c$. On the other hand, in the limit $\beta \to 0$, Eq. (8) yields the local dispersion relation for shear Alfven waves.

Substituting Eq. (6) into Eg. (7), we obtain

$$\left[\frac{\partial^2}{\partial t^2} + (\vec{k}\cdot\vec{B}_o)^2\frac{v_A^2}{B_o^2}\right]\nabla^2\xi_{1y} + \left(\frac{\partial\xi_{1y}}{\partial y}\right)\frac{v_A^2}{B_o^2}\frac{d}{dy}[(\vec{k}\cdot\vec{B}_o)^2] + \frac{k^2 g}{r_n}\xi_{1y} = 0 \tag{10}$$

where $(\vec{k}\cdot\vec{B}_o) = B_o(k_z + K_x y/L_s)$. We solve this equation subject to the initial condition

$$\xi_{1y}(y,0) = \exp(iu_o ky - k^2y^2), \tag{11}$$

where u_o is a dimensionless parameter measuring the inclination of the initial wave packet in the x-y plane. The gaussian envelope of the wave-packet [Eq. (11)] assures that all solutions remain bounded as $|y| \to \infty$. We further assume that this initial wavelet is moving in the +x direction.

In terms of the dimensionless space and time variables (s,τ) defined by

$$\tau = (v_A t/L_s)k_x/(k_x^2 + k_z^2)^{1/2}, \tag{12}$$

$$s = (k_x^2 + k_z^2)^{1/2}(y + L_s k_z/k_x), \tag{13}$$

Eq. (10) can be expressed as

$$\left(\frac{\partial^2}{\partial\tau^2} + s^2\right)\left(\frac{\partial^2\xi}{\partial s^2} - \xi\right) + 2s\frac{\partial\xi}{\partial s} + \frac{\beta}{\beta_c}\xi = 0. \tag{14}$$

In Eq. (14), $\xi \equiv \xi_{1y}(s,\tau)$, and β and β_c are defined in Eq. (9). The initial condition in Eq. (11) can then be expressed as

$$\xi(s,0) = \exp(iu_o s - s^2), \tag{15}$$

where we have set $k_z = 0$ without loss of generality.

As shown below, the evolution of the initial wavepacket in Eq. (15) can readily be studied in terms of the spectral transform $z(u,\tau)$, where $z(u,\tau)$ is related to $\xi(s,\tau)$ by

$$\xi(s,\tau) = \int_{-\infty}^{\infty} du\, z(u,\tau)\exp(ius). \tag{16}$$

The equation governing the solution of $z(u,\tau)$ is

$$\frac{\partial^2 z}{\partial \tau^2} = \frac{1}{1+u^2}\frac{\partial}{\partial u}\left[(1+u^2)\frac{\partial z}{\partial u}\right] + \frac{(\beta/\beta_c)}{1+u^2} z \ . \tag{17}$$

Moreover, the initial condition in Eq. (15) transforms according to

$$z(u,0) = \exp[-(u-u_o)^2/4\,], \tag{18}$$

which represents a gaussian pulse centered at u_o. This pulse is assumed to travel at the -u direction at time $\tau = 0$.

We note here an interesting relationship between $z(u,\tau)$ and $\xi(s,\tau)$. If β is sufficiently large, we expect a localized, purely growing, ballooning mode to be excited. In such a case, the eigenmode solution

$$\xi(s,\tau) = \exp(\Gamma\tau)\psi(s) \tag{19}$$

has a corresponding spectral solution

$$z(u,\tau) = \exp(\Gamma\tau)Z(u), \tag{20}$$

where Γ is the normalized growth rate of the eigenmode solution $\psi(s)$. Substituting Eqs. (19) and (20) into Eqs. (14) and (17), the following equations are readily obtained:

$$\frac{d}{ds_1}\left[(1+s_1^2)\frac{d\psi}{ds_1}\right] + \left[\frac{\beta}{\beta_c} - \Gamma^2(1+s_1^2)\right]\psi = 0, \tag{21}$$

$$\frac{d}{du}\left[(1+u^2)\frac{dZ}{du}\right] + \left[\frac{\beta}{\beta_c} - \Gamma^2(1+u^2)\right]Z = 0, \tag{22}$$

where $s_1 = s/\Gamma$. Note from Eqs. (21) and (22) that the eigenmode solution $\psi(s)$ and its Fourier transform $Z(u)$ are governed by the same equation. It then follows that if $z(u,\tau)$ evolves to an eigenmode solution in the spectral space u, it is also the eigenmode solution in the real space s, after appropriate scaling. Therefore, in the following, it is sufficient to investigate the evolution of the spectrum $z(u,\tau)$ from Eqs. (17) and (18).

III. NUMERICAL RESULTS

In this section we summarize numerical studies of the evolution of the spectrum $z(u,\tau)$ making use of Eqs. (17) and (18). We first consider the case $\beta = 0$, and subsequently investigate cases with $\beta > 0$. It is assumed that $u_o = 20$ in all of the numerical calculations.

(a) $\beta = 0$:

In this case, the ballooning effect is absent, and Eq. (17) reduces to

$$\frac{\partial^2 z}{\partial \tau^2} = \frac{1}{1+u^2} \frac{\partial}{\partial u} \left[(1 + u^2) \frac{\partial z}{\partial u} \right]. \tag{23}$$

This equation[6] is identical to the equation governing sound propagation in a diverging tube with variable cross-sectional area $S = 1 + u^2$, where u is the distance along the tube. The evolution of the spectrum $z(u,\tau)$ is therefore identical to the evolution of the initial "sound pulse" $z(u,o)$ in such a tube (Fig. 1). Transient amplification of such a sound pulse is possible as the sound pulse reaches the region near $u = 0$. Note from Eq. (23) that the speed of propagation $du/d\tau$

of the sound pulse is equal to unity.

The detailed evolution of the spectrum $z(u,\tau)$ is shown in Fig. 2 for the case of $u_o = 20$. The initial pulse has unit amplitude at $\tau = 0$, centered at $u_o = 20$. By time $\tau = 10$, the pulse is centered at $u = 10$ and the amplitude is amplified by a factor of 2. This can be simply interpreted from Fig. 1, i.e., the cross-sectional area S of the tube at $u = 20$ is 4 times that at $u = 10$.

The sound pulse is then scattered at a later time as it approaches the narrowest region of the tube (near $u \simeq 0$ in Fig. 1) between $\tau = 18$ and $\tau = 22$. Subsequently, the sound pulse divides into two pulses that travel to $u \to \pm\infty$ with diminishing amplitudes. For $u_o = 20$, it is evident from Fig. 2 that the amplitude of the wavepacket increases by a factor of 10 at maximum. On the other hand, if the sound pulse is initially centered at $u_o = 100$, the amplitude gain would be approximately 50 as the pulse reaches $u = 0$. This is in qualitative agreement with the estimate given in Ref. 6. The nature of this transient amplification has been discussed in Sec. I and is analogous to that encountered in classical hydrodynamic shear flow[11].

(b) $\beta > 0$:

The evolution of the spectrum for the cases $\beta/\beta_c = 0.5$, 0.75, 1, and 1.1 is shown in Figs. 3 - 6, respectively. Note that the effect of curvature on the evolution of the shear Alfven waves becomes increasingly important for finite values of beta. These solutions are obtained by solving Eqs. (17) and (18) numerically. In Figs. 3 - 6, the initial spectrum $z(u,o)$ is given by Eq.(18) with $u_o = 20$. During the time

interval between $\tau = 0$ and $\tau = 10$, the spectrum $z(u,\tau)$ is nearly identical for all the cases shown in Figs. 3 - 6. This is because Eq. (23) is a good approximation to Eq. (17) during this time interval.

For $\beta/\beta_c = 0.5$, it is evident from Fig. 3 that ballooning effects only slightly enhance the amplification of the shear Alfven wave in comparison with the case $\beta/\beta_c = 0$ (Fig. 2). In both cases, the peak amplification factor is approximately 10 (compared with the initial value), and the solutions decay at large times.

For $\beta/\beta_c = 0.75$ (Fig. 4), a weak ballooning mode develops from the initial shear Alfven wave by time $\tau = 30$. Note that the spectrum $z(u,\tau)$ during the interval from $\tau = 0$ to $\tau = 18$ is similar to the case $\beta/\beta_c = 0.5$ (Fig. 3). For $\beta/\beta_c = 0.75$, the amplitude gain at $\tau = 30$ is approximately 70.

For $\beta/\beta_c = 1$ (Fig. 5), a moderately strong ballooning mode has already developed by $\tau = 30$. Prior to $\tau = 18$, the perturbation is essentially a pure shear Alfven wave. Moreover, the amplitude gain at $\tau = 30$ is approximately 680.

For $\beta/\beta_c = 1.1$ (Fig. 6), a very strong ballooning mode appears, and the amplitude gain is about 1450 at $\tau = 30$. Comparing the peak amplitudes of $z(u,\tau)$ at $\tau = 22$ and at $\tau = 30$, we estimate that the growth rate of this mode is $\gamma = 0.36\ v_A/L_s$. This is in qualitative agreement with that obtained from the local dispersion relation in Eq. (8). In particular, if we approximate $k_{\|}$ by $1/L_s$ in Eq. (8), the local growth rate is approximately $\gamma_L \simeq 0.31\ v_A/L_s$ for $\beta/\beta_c = 1.1$.

In summary, in Figs. 4 - 6, the initial perturbation evolves into a ballooning mode by time $\tau = 30$. Figures 4 - 6 illustrate the spectrum $Z(u)$ of the eigenmodes at various values of τ. Moreover, as shown at the end of Sec. II, for large τ this also corresponds to $\psi(s)$ in configuration space.

IV. CONCLUSIONS

In this paper, we have studied the transient amplification of shear Alfven waves and their development into the ballooning instabilities as the plasma pressure is increased. The analysis has made use of an ideal MHD description in slab geometry. The evolutionary process described by such a simplified model is expected to be qualitatively valid when applied to toroidal geometry. The main results of our numerical study of the evolution of an initial wavepacket can be summarized as follows. In the limit $\beta \to 0$, the transient amplification of shear Alfven waves confirms previous results[6]. For $\beta < \beta_c/2$, this transient amplification is not significantly altered. For $\beta \gtrsim 0.75\beta_c$, however, ballooning effects dominate the evolution of the shear Alfven waves, and substantial amplification is observed. Indeed, for $\beta \gtrsim 1.1\beta_c$, the initial shear Alfven waves develop into a highly unstable, localized, ballooning mode.

ACKNOWLEDGEMENTS

This work is supported in part by the National Science Foundation and in part by the Department of Energy.

REFERENCES

1. J. D. Callen, Phys. Rev. Lett. 39, 1540 (1977).
2. A. B. Rechester and M. N. Rosenbluth, Phys. Rev. Lett. 40, 38 (1978).
3. K. Molvig, J.E. Rice and M.S. Tekula, Phys. Rev. Lett. 41, 1240 (1978).
4. J.F. Drake, N.T. Gladd, C.S. Liu and C.L. Chang, Preprint PL #79-026, University of Maryland, College Park, Maryland (1979).
5. S.J. Sweben, C.R. Menyuk and R.J. Taylor, Phys. Rev. Lett. 42, 1270 (1979).
6. Y. Y. Lau, Phys. Rev. Lett. 42, 779 (1979).
7. S. P. Hirshman and K. Molvig, Phys. Rev. Lett. 42, 648 (1979).
8. D. W. Ross and S. M. Mahajan, Phys. Rev. Lett. 40, 324 (1978).
9. K.T. Tsang, P.J. Catto, J.C. Whitson and T. Smith, Phys. Rev. Lett. 40, 327 (1978).
10. T. M. Antonsen, Phys. Rev. Lett. 42, 708 (1978).
11. W. McF. Orr, Proc. Roy. Irish Acad. A27, 69 (1907).
12. H. Grad, Phys. Today 22, 34 (1969).
13. W. Grossman and J.A. Tataronis, Z. Physik 261, 203 and 217 (1973).
14. L. Chen and A. Hasegawa, Phys. Fl. 17, 1399 (1974).
15. P. L. Pritchett and J. M. Dawson, Phys. Fl. 21, 516 (1978).
16. B. Coppi, Phys. Rev. Lett. 39, 939 (1977) and references therein.
17. B. Coppi, A. Ferreira, J.W.K. Mark and J.J. Ramos, Comments on Plasma Physics and Controlled Fusion, in press (1979).
18. C. Mercier, paper CN-37-p-3-2 and L.E. Zakharov, paper CN-37-p-3-1, in Plasma Physics and Controlled Nuclear Fusion Research (International Atomic Energy Agency, Vienna, 1978).

FIGURE CAPTIONS

Fig. 1. An initial sound pulse $z(u,o)$ in a diverging tube. The corss-sectional area $S = 1 + u^2$ is a function of the distance u along the tube.

Fig. 2. Evolution of the spectrum of shear Alfven waves without ballooning effects ($\beta = 0$).

Fig. 3. Evolution of the spectrum of shear Alfven waves for $\beta/\beta_c = 0.5$.

Fig. 4. Development of the shear Alfven waves into a ballooning mode for $\beta/\beta_c = 0.75$.

Fig. 5. Same as Fig. 4, with $\beta/\beta_c = 1$.

Fig. 6. Same as Fig. 4, with $\beta/\beta_c = 1.1$.

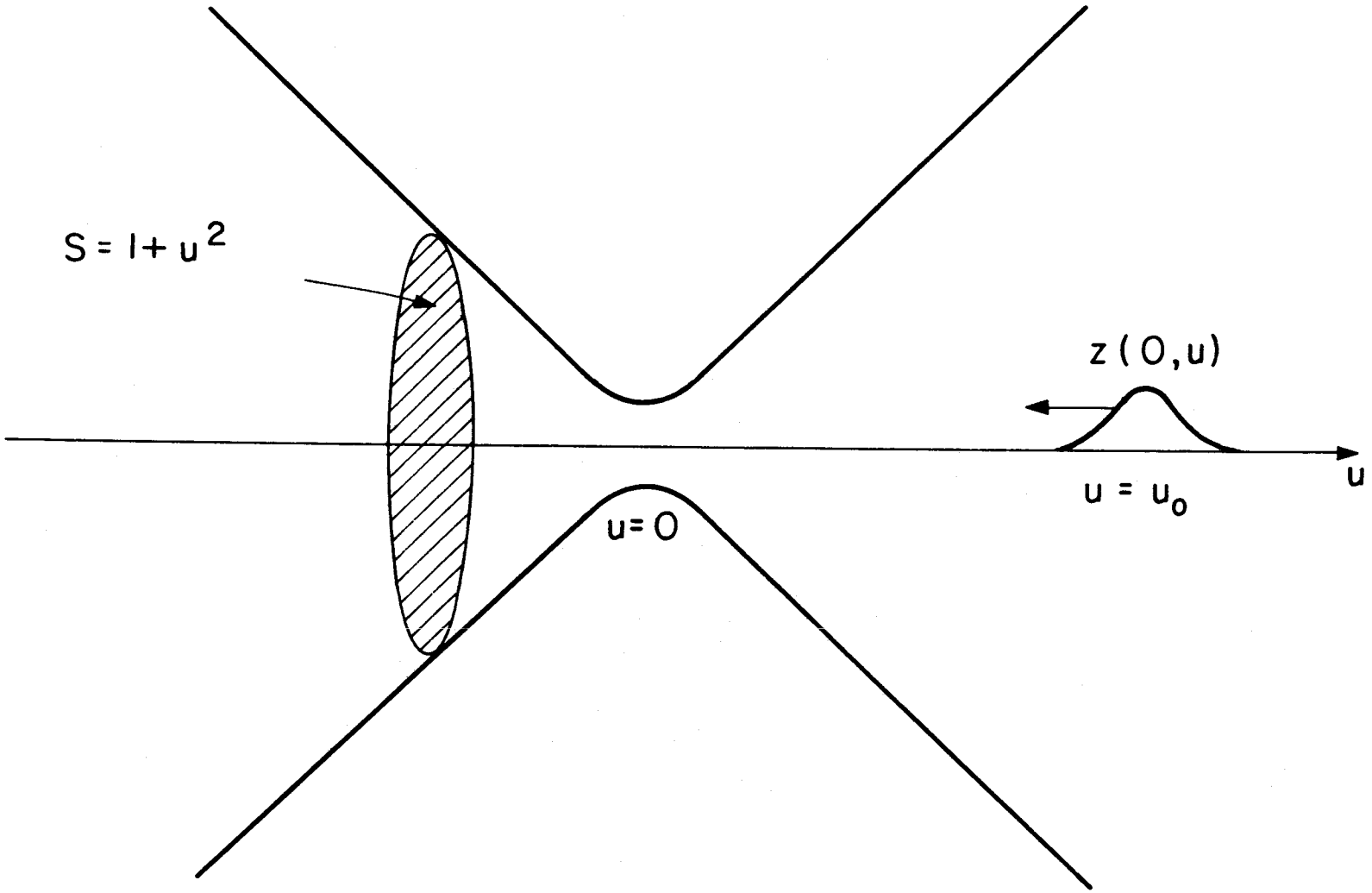
S = 1+ u 2
z (0, u)
u
u = u0
u= 0

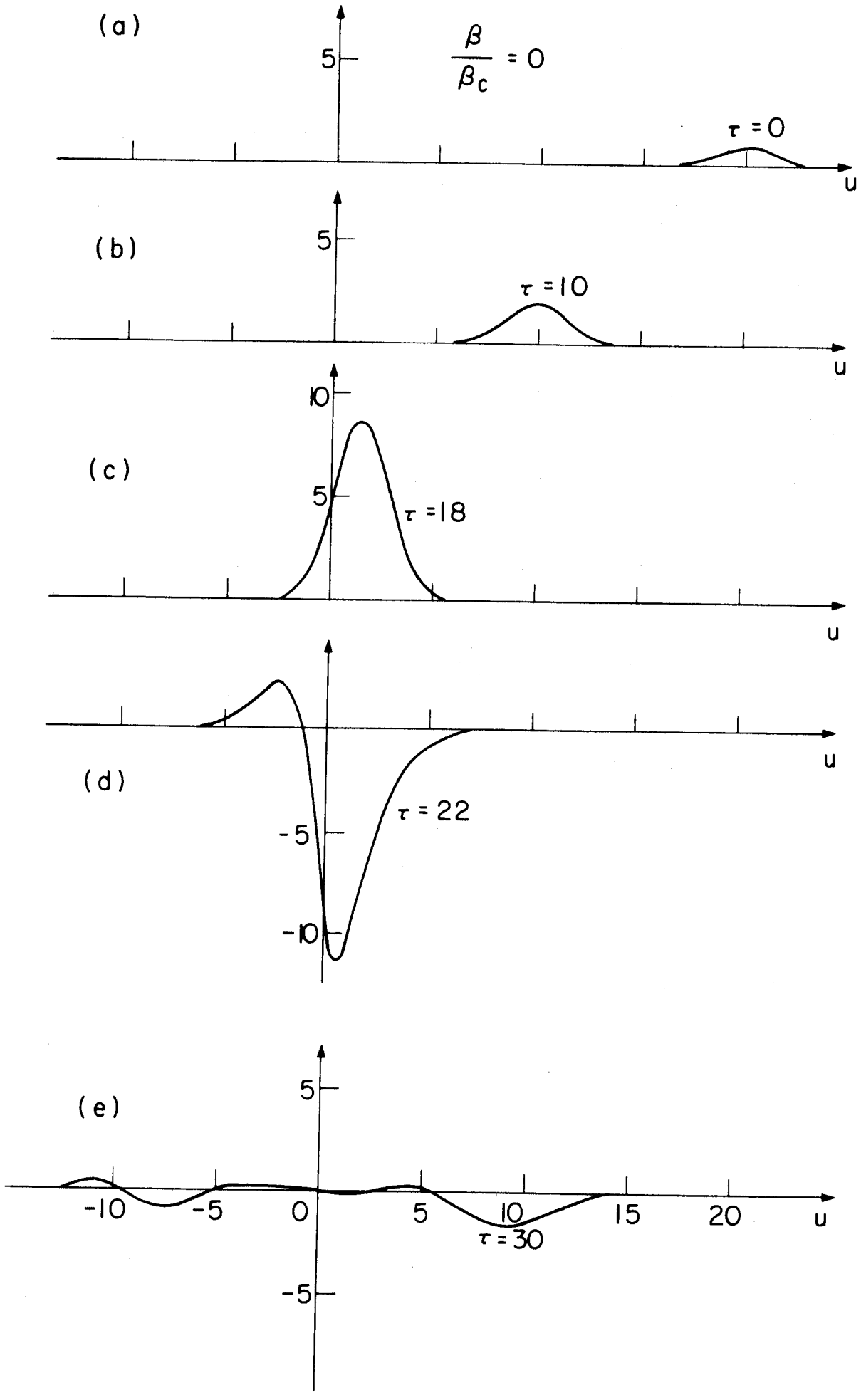
(a)
$\frac{\beta}{\beta_c} = 0$
5
$\tau = 0$
u
(b)
5
$\tau = 10$
u
(c)
10
5
$\tau = 18$
u
(d)
$\tau = 22$
-5
-10
u
(e)
5
-10
-5
0
5
10
15
20
u
$\tau = 30$
-5

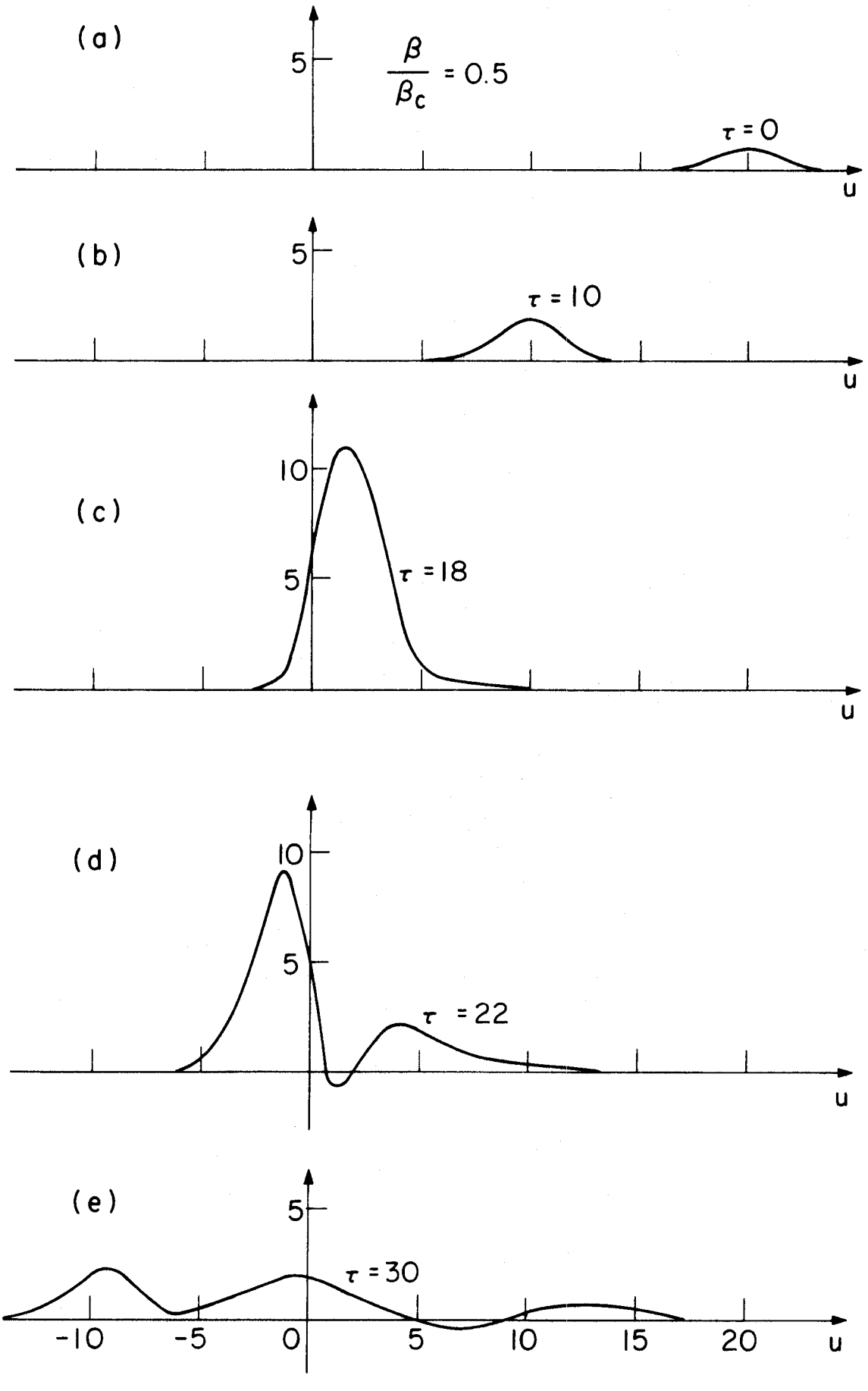
(a)
5
$\frac{\beta}{\beta_c} = 0.5$
$\tau = 0$
u
(b)
5
$\tau = 10$
u
(c)
10
5
$\tau = 18$
u
(d)
10
5
$\tau = 22$
u
(e)
5
$\tau = 30$
-10
-5
0
5
10
15
20
u

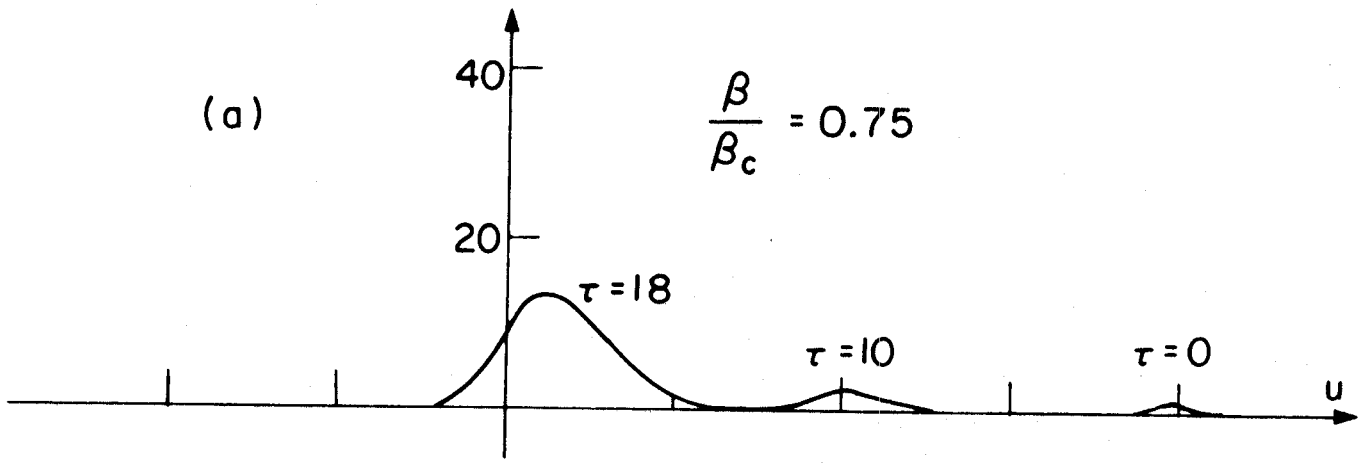
(a)
40
20
$\frac{\beta}{\beta_c} = 0.75$
$\tau = 18$
$\tau = 10$
$\tau = 0$
u

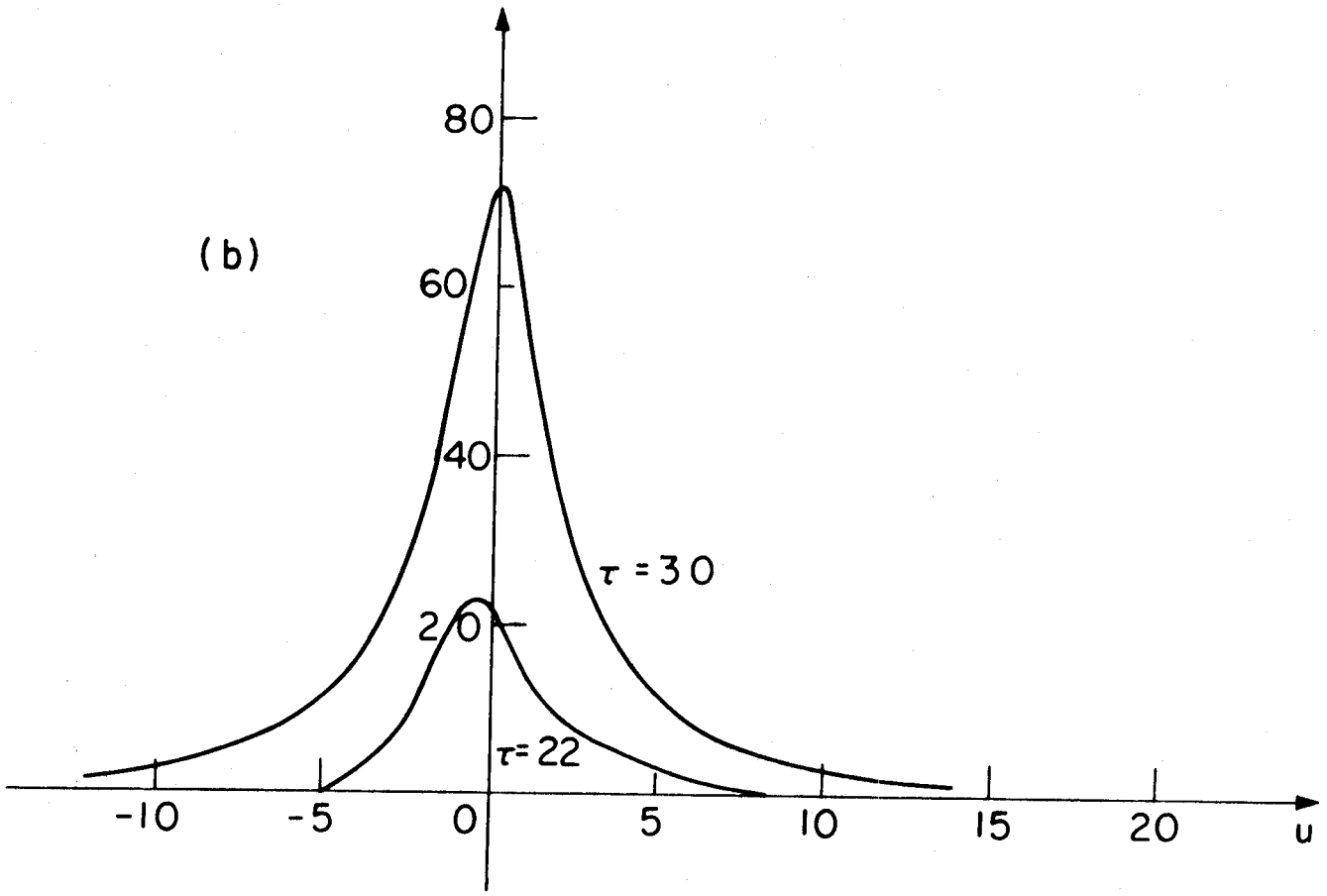
(b)
80
60
40
20
$\tau = 30$
$\tau = 22$
-10
-5
0
5
10
15
20
u

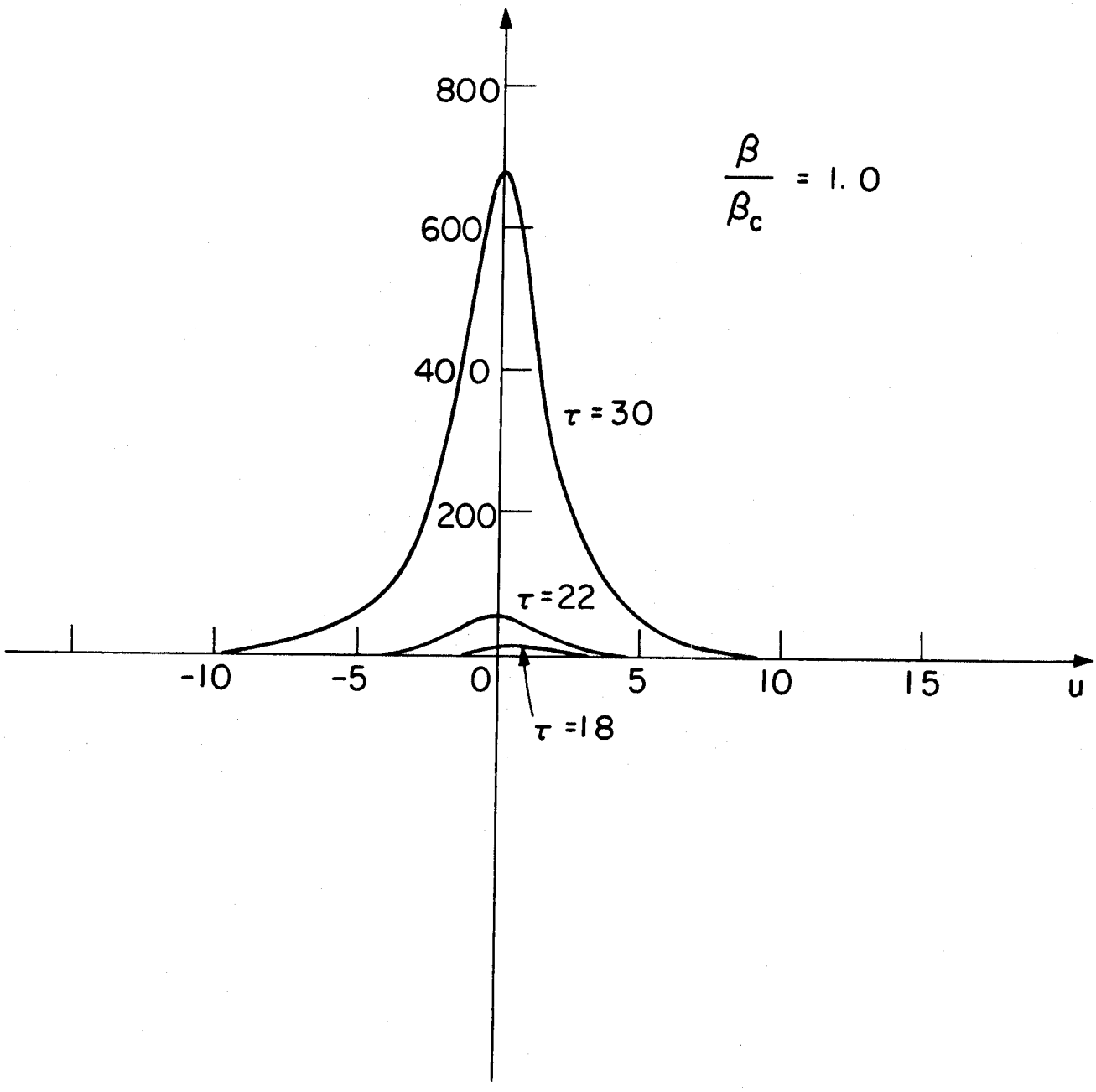
800
600
400
200
$\frac{\beta}{\beta_c} = 1.0$
$\tau = 30$
$\tau = 22$
$\tau = 18$
-10
-5
0
5
10
15
u

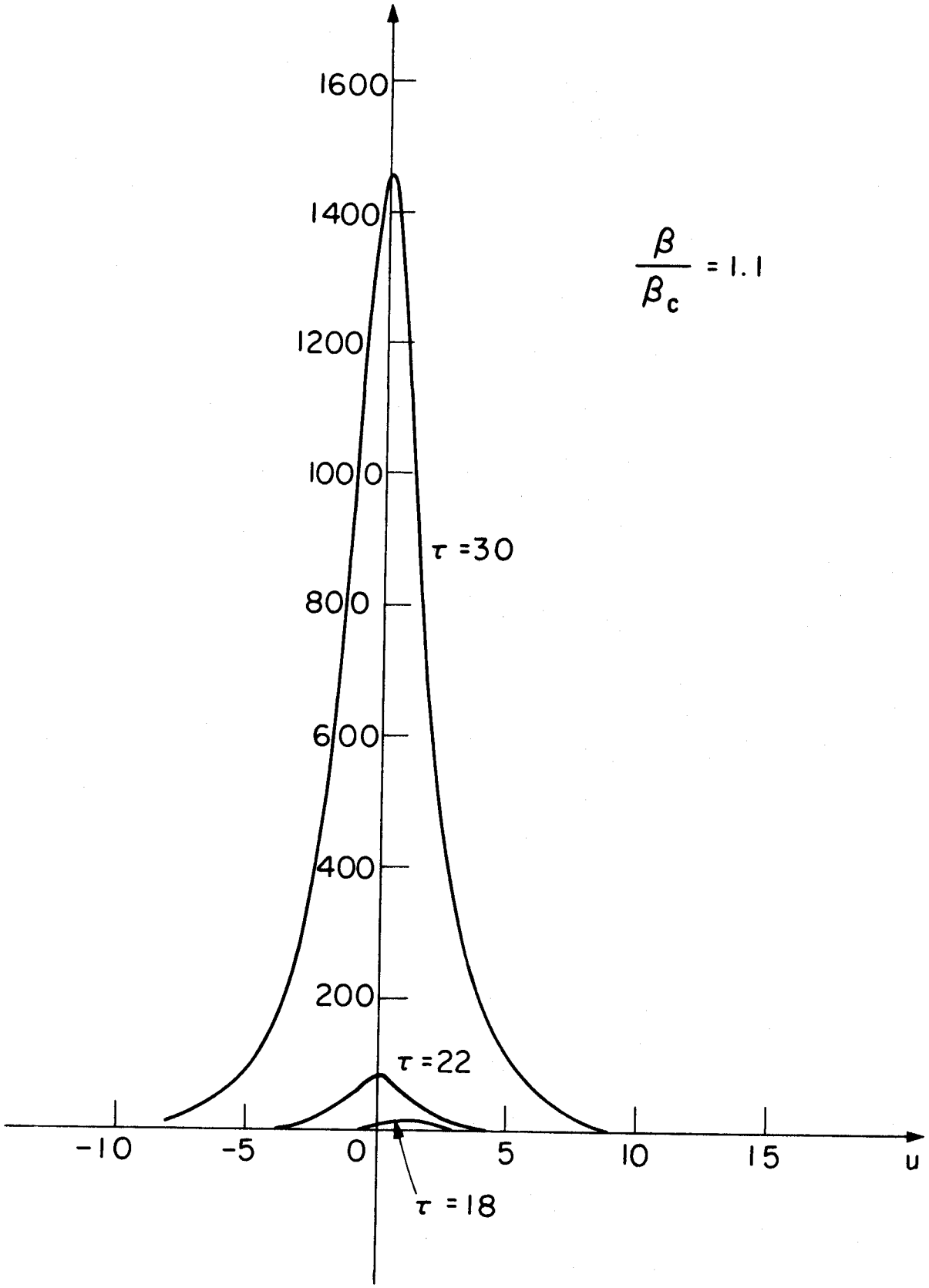
1600
1400
1200
1000
800
600
400
200
$\frac{\beta}{\beta_c} = 1.1$
$\tau = 30$
$\tau = 22$
$\tau = 18$
-10
-5
0
5
10
15
u